A MOLECULAR DYNAMICS DERIVED FINITE ELEMENT METHOD FOR STRUCTURAL SIMULATIONS AND FAILURE OF GRAPHENE NANOCOMPOSITES

A. A. R. Wilmes[1*], S. T. Pinho[1]

[1]*Department of Aeronautics, Imperial College London, South Kensington Campus, London SW7 2AZ*
**andre.wilmes07@imperial.ac.uk*

Keywords: MDFEM, FEM, AFEM, Fracture.

Abstract
The recent rise of 2D materials, such as graphene, has expanded the interest in nano-electromechanical systems (NEMS). The increasing ability of synthesizing more exotic NEMS architectures, creates a growing need for a cost-effective, yet accurate nano-scale simulation method. Established methodologies like Molecular Dynamics (MD) trail behind synthesis capabilities because the computational effort scales quadratically. The equilibrium equations of MD are equivalent with those of the computationally more favourable Finite Element Method (FEM). However, current implementations exploiting this equivalence remain limited due to the FEM iterative solvers requiring a large number of lengthy force field derivatives and specifically tailored element topologies. This paper proposes a merged Molecular Dynamic Finite Element Method (MDFEM) which does not require the manual derivation of these derivatives. Hence, implementing MDFEM-specific element topologies is straight-forwards and thus, different non-linear MD force field potentials can be solved exactly within the FEM, at reduced computational costs. The proposed multi-scale and multi-physics compatible MDFEM is equivalent to the MD, as demonstrated firstly by an example of brittle fracture in Carbon Nanotubes (CNT), and secondly by conformational analyses on Non-Equilibrium initial meshes of Pillared Graphene Structures (PGS).

1 Introduction

Simulating the mechanical response of nano-structures is important for a wide and rapidly increasing range of areas. Continuous progress in nano-synthesis capabilities, together with graphene's first applications in nano-electromechanical systems (NEMS) [1], have further spurred interest in efficient, robust and flexible numerical nano-simulation methods. One of the main challenges for nano-simulation models consists of achieving a suitable balance between the accuracy of the physical representation and the scale of applicability. At one extreme, *Ab Initio* simulations, based on Density Functional Theory (DFT), can offer high accuracy but cannot readily be used for domains beyond $\mathcal{O}(10^2)$ atoms. At the other extreme, classical Molecular Mechanics (MM) and Dynamics (MD) methods [2] only resolve nuclei motion (Born-Oppenheimer approximation), but may be typically applied to domains with $\mathcal{O}(10^9)$ atoms [3]. A variety of intermediate theory levels have emerged such as the hybrid DFT-MD Car-Parrinello method [4], or the reactive MD force fields [5].

The MD method has increasingly been incorporated in the Finite Element Method (FEM) framework [6-11] as the equilibrium equations of MD and FEM may be expressed in equivalent forms. The resulting Atomistic Finite Element Method (AFEM) [8], also named Molecular Dynamic Finite Element Method (MDFEM) [12], is both computationally more favourable than MD [8], and offers a significant increase in compatibility and integrability with larger scale continuum FEM simulations. Several comprehensive presentations and reviews of AFEM/MDFEM and its implementations are available [8, 12-14].

Nonetheless, MDFEM remains a non-consolidated method because formal derivations are scarce, with significant differences arising on the topologies of the required MDEFM-specific elements. The available MDFEM element designs vary considerably in complexity and their implementation is often not straight-forward [8-10]. Additionally, only few proposed MDFEM element topologies are fully non-linear and non-local capable. This has led to MDFEM often being implemented using readily available, standard structural FEM elements such as beams, trusses and springs [6, 7, 11], which results in detrimental restrictions of MDFEM's full non-linear capabilities. This paper presents a fully non-linear MDFEM model, based on appropriate and comprehensive MDFEM-specific element topologies.

2 Equilibrium Equations: From Hamilton over Lagrange to a Discrete FEM

A variational statement of equilibrium for a particle domain, Ω, can formally be derived from Hamilton's principle, which subjected to a Legendre transform, leads to Lagrange's equation. In the framework of Newtonian mechanics, the dynamic equilibrium of Ω, without damping, may be hence stated as:

$$\mathbf{M}\ddot{\mathbf{u}} + \left(\mathbf{J}_{\mathbf{u}}^{V}\right)^{\mathrm{T}} = \mathbf{f}, \tag{1}$$

where $\mathbf{u} \in \mathbb{R}^{n\times 1}$ denotes the n generalized coordinates of the system, chosen to be the translational displacements of all particles in a global Cartesian coordinate system. Thus, the generalized corresponding forces, denoted $\mathbf{f} \in \mathbb{R}^{n\times 1}$, are a set of linear forces only and the mass matrix, $\mathbf{M} \in \mathbb{R}^{n\times n}$, is diagonal. $\mathbf{J}_{\mathbf{u}}^{V} \in \mathbb{R}^{1\times n}$ represents the Jacobian of the conservative potential field, V, which governs Ω, relative to the generalized coordinates $\mathbf{u}$.

The rest state of Ω, when $\mathbf{u} = \mathbf{u}_0 = \mathbf{0}$, is defined by the atoms' equilibrium positions, denoted by $\mathbf{x} \in \mathbb{R}^{n\times 1}$. Any deformed state of Ω may therefore be described by $\mathbf{r} = \mathbf{x} + \mathbf{u}$ (figure 1).

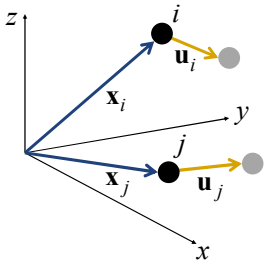

Figure 1. Coordinate System and Displacements Definitions for Atoms i and j

Equation (1) is typical for a FEM framework and can be solved using a Newton-Raphson scheme provided the Hessian of the potential can be determined, which is expressed as:

$$\mathbf{H}_{\mathbf{u}}^{V} = \frac{\partial}{\partial \mathbf{u}}\left(\frac{\partial V}{\partial \mathbf{u}^{\mathrm{T}}}\right). \tag{2}$$

3 Molecular Force Fields

3.1 Constituent Sub-Potentials

In general, a molecular force field, V, consists of the superposition of sub-potentials, V_S, as:

$$V(\mathbf{c}) = \sum_{\mathbb{S}} V_S(\mathbf{c}_S), \tag{3}$$

where $\mathbb{S}$ represents the set of included sub-potentials, $\mathbf{c} \in \mathbb{R}^{m\times 1}$ and $\mathbf{c}_S \in \mathbb{R}^{m_S\times 1}$ denote the m and m_S specific characteristic variables (e.g. bond lengths and angles) required for evaluating V and V_S respectively. Both non-reactive (e.g. MM3 [15], Lobo-Keating [16]) and reactive force fields (e.g. Brenner [5]) may be expressed in the form of equation (3).

3.2 Characteristic Variables

The characteristic variables, $\mathbf{c}$, may always be expressed as $\mathbf{c} = \mathbf{c}(\mathbf{x},\mathbf{u})$, so that it is possible to reformulate the potential explicitly as:

$$V(\mathbf{c}(\mathbf{x},\mathbf{u})) = \sum_{\mathbb{S}} V_S(\mathbf{c}_S(\mathbf{x},\mathbf{u})) = \sum_{\mathbb{S}} V_S(\mathbf{x},\mathbf{u}). \tag{4}$$

Figure 2 outlines a selection of common characteristic variables. A comprehensive literature covers such variable-defining sketches and the reader is referred to [17] for a good collection.

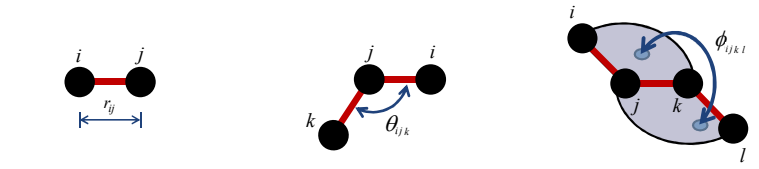

(a) Bond Stretching *(b) Bond Bending* *(c) Bond Torsion*

Figure 2. Characteristic Variables of Force Field Potentials

4 Molecular Dynamic Finite Element Method

4.1 Constituent Sub-Jacobians, Sub-Hessians and their Symbolic Derivation

Taking advantage of the sub-potential nature of force fields, equation (3) and noting that for each sub-potential, V_S, the corresponding sub-domain, Ω_S, may in turn be divided into p_S partitions, Ω_S^i, (figure 3), where $V_S^i \equiv V_S$ in partition Ω_S^i and is zero elsewhere, the total domain's potential V, may be then stated as:

$$V(\mathbf{x},\mathbf{u}) = \sum_{\mathbb{S}}\sum_{i}^{p_S} V_S^i\left(\mathbf{c}_S^i(\mathbf{x}_S^i,\mathbf{u}_S^i)\right) = \sum_{\mathbb{S}}\sum_{i}^{p_S} V_S^i(\mathbf{x}_S^i,\mathbf{u}_S^i), \tag{5}$$

where $\mathbf{x}_S^i \in \mathbb{R}^{n_S\times 1}$ and $\mathbf{u}_S^i \in \mathbb{R}^{n_S\times 1}$ are the n_S entries of $\mathbf{x}$ and $\mathbf{u}$ required for evaluating V_S^i.

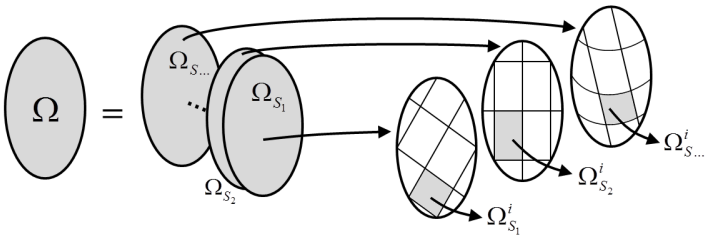

Figure 3. Illustration of Domain Decomposition and Sub-Domain Partitioning

It follows naturally that an element topology may be created for each individual sub-potential, V_S, which is able to supply the necessary characteristic variables $\mathbf{c}_S^i\left(\mathbf{x}_S^i,\mathbf{u}_S^i\right)$ in partition Ω_S^i, and which is in turn meshed p_S times on the sub-domain Ω_S. $\mathbf{J}_\mathbf{u}^V$ and $\mathbf{H}_\mathbf{u}^V$ in equations (1) and (2) may be hence obtained by, first evaluating the sub-potentials' Jacobian and Hessian $\mathbf{J}_{\mathbf{u}_S^i}^{V_S^i}$ and $\mathbf{H}_{\mathbf{u}_S^i}^{V_S^i}$, in all sub-domain partitions Ω_S^i, followed by assembling processes of the type:

$$\mathbf{J}_\mathbf{u}^V\left(\mathbf{x},\mathbf{u}\right)=\sum_{\mathbb{S}}\sqcup_{p_S}^{V_S}\left(\mathbf{J}_{\mathbf{u}_S^i}^{V_S^i}\left(\mathbf{x}_S^i,\mathbf{u}_S^i\right)\right)=\sum_{\mathbb{S}}\mathbf{J}_\mathbf{u}^{V_S}\left(\mathbf{x},\mathbf{u}\right), \tag{6}$$

$$\mathbf{H}_\mathbf{u}^V\left(\mathbf{x},\mathbf{u}\right)=\sum_{\mathbb{S}}\sqcup_{p_S}^{V_S}\left(\mathbf{H}_{\mathbf{u}_S^i}^{V_S^i}\left(\mathbf{x}_S^i,\mathbf{u}_S^i\right)\right)=\sum_{\mathbb{S}}\mathbf{H}_\mathbf{u}^{V_S}\left(\mathbf{x},\mathbf{u}\right), \tag{7}$$

where $\sqcup_{p_S}^{V_S}$ denotes the assembly operator which assembles the contributions of all p_S Jacobians, $\mathbf{J}_{\mathbf{u}_S^i}^{V_S^i}\left(\mathbf{x}_S^i,\mathbf{u}_S^i\right)\in\mathbb{R}^{1\times n_S}$, into the corresponding positions within $\mathbf{J}_\mathbf{u}^{V_S}\left(\mathbf{x},\mathbf{u}\right)\in\mathbb{R}^{1\times n}$ and similarly the contributions of all p_S Hessians, $\mathbf{H}_{\mathbf{u}_S^i}^{V_S^i}\left(\mathbf{x}_S^i,\mathbf{u}_S^i\right)\in\mathbb{R}^{n_S\times n_S}$ into $\mathbf{H}_\mathbf{u}^{V_S}\left(\mathbf{x},\mathbf{u}\right)\in\mathbb{R}^{n\times n}$. The numerical solution to the global equilibrium problem, equation (1), using an iterative solution scheme requiring the Hessian, equation (2), can therefore be obtained trivially using equations (6) and (7) together with suitable element topologies. Modern interpreted processing languages (e.g. MATLAB), capable of rapid symbolic derivation of analytical expressions, can generate the elements' Jacobian, $\mathbf{J}_{\mathbf{u}_S^i}^{V_S^i}$, and Hessian, $\mathbf{H}_{\mathbf{u}_S^i}^{V_S^i}$, symbolically.

4.2 Element Topologies

The element topology required for each sub-potential is determined by the respective components of $\mathbf{c}_S^i$, so that the most compact and comprehensive element designs are identical to the characteristic variable-defining sketches for each force field (figure 2). Elements for reactive force fields include more atoms than those elements used for non-reactive potentials (figure 4) because the reactive bond-order characteristic has a higher non-locality.

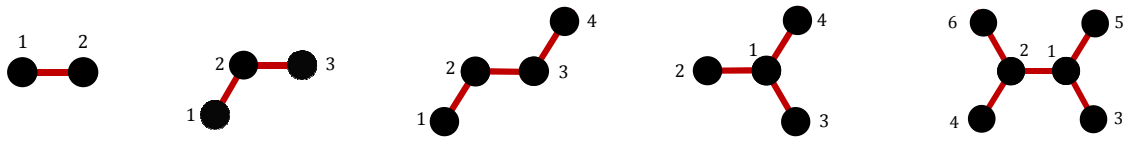

(a) NR-2 *(b) NR-3* *(c) NR-4-C* *(d) NR-4-S* *(e) R-6*

Figure 4. Selection of Non-Reactive (NR) and Reactive (R) Topologies

A small selection of characteristic variables, which the elements in figure 4 can supply and for which sub-potentials they may be required, is outlined in table 1.

NR-2	**NR-3**	**NR-4-C**	**NR-4-S**
$r_{12}=\sqrt{\mathbf{r}_{12}\cdot\mathbf{r}_{12}}$	$r_{21}=\sqrt{\mathbf{r}_{21}\cdot\mathbf{r}_{21}}$	$\cos\left(\phi_{1234}\right)=-\hat{\mathbf{r}}_{123}\cdot\hat{\mathbf{r}}_{234}$	$\mathbf{d}_1=\mathbf{r}_{12}+\mathbf{r}_{13}+\mathbf{r}_{14}$
$r_{12}^2=\mathbf{r}_{12}\cdot\mathbf{r}_{12}$	$\left(r_{21}r_{23}\cos\left(\theta_{123}\right)\right)=\mathbf{r}_{21}\cdot\mathbf{r}_{23}$	$\hat{\mathbf{r}}_{123}=\left(\frac{\mathbf{r}_{12}\times\mathbf{r}_{23}}{r_{12}r_{23}}\right)$	$d_1^2=\mathbf{d}_1\cdot\mathbf{d}_1$
$V_\mathrm{S},V_\mathrm{VDW}$	$V_\mathrm{B},V_\mathrm{SB},V_\mathrm{SS}$	$V_\mathrm{T},V_\mathrm{TS},V_\mathrm{TB}$	$V_\mathrm{I},V_\mathrm{IT},V_\mathrm{BB}$

S = Stretch, B = Bend, T = Torsion, I = Inflexion, IT = Improper Torsion, SS = Stretch-Stretch
SB = Stretch-Bend, BB = Bend-Bend, TS = Torsion-Stretch, TB = Torsion-Bend, VDW = Van der Waals

Table 1. Element Topologies, Characteristic Variables, $\mathbf{c}_S$, and Applicable Sub-Potentials, V_S.

5 Applications

Two applications of the implemented MDFEM are presented. Firstly, the equivalence of MDFEM and MD is demonstrated using a static, non-linear fracture simulation of CNT. Secondly, non-equilibrium meshes of complex three-dimensional Pillared Graphene Structures (PGS) are allowed to relax, hence demonstrating the current implementation's capability to perform full conformational analyses.

5.1 Brittle Failure of Carbon Nanotubes (CNT) with Defects

The MD study by Belytschko et al. [18], investigating the effects of defects on the fracture behaviour of CNT, was chosen as a reference to demonstrate the equivalence of MDFEM and MD in a highly non-linear environment up to, and including bond failure. Three CNT configurations (table 2) were tested in a static analysis, $\ddot{\mathbf{u}} = \mathbf{0}$, and were strained axially to fracture. The effect of defects was included by softening a single bond in the middle of the CNT by 10% (i.e. effectively a 0.9 multiplication factor was applied to both $\mathbf{J}^{V_S^i}_{\mathbf{u}_S^i}$ and $\mathbf{H}^{V_S^i}_{\mathbf{u}_S^i}$ of the affected elements). Following Belytschko et al. [18], the reactive bond-order Brenner potential [5], is approximated in this example by a Morse type potential of the form:

$$V = V_{\mathrm{S}} + V_{\mathrm{B}} = \alpha\left\{\left[1 - e^{-\beta\left(r_{ij} - r_0\right)}\right]^2 - 1\right\} + \frac{1}{2}\gamma\left(\theta_{ijk} - \theta_0\right)^2\left[1 + \lambda\left(\theta_{ijk} - \theta_0\right)^4\right]. \tag{8}$$

The above potential was developed to be equivalent to the Brenner force field for strains up to 10%, but without suffering from the subsequent *camel-back* problem in the force-displacement relation. The fitting constants for equation (8) are: $r_0 = 1.39\,\text{Å}$, $\theta_0 = 2.094\,\text{rad}$, $\alpha = 6.03105\,\text{nN Å}$, $\beta = 2.625\,\text{Å}^{-1}$, $\gamma = 9.0\,\text{nN Å/rad}^2$ and $\lambda = 0.754\,\text{rad}^{-4}$ [18]. The present formulation identifies CNT uniquely by a triplet of integers, such as $(20,0,10)$. The first two indices, $(20,0)$, refers to the commonly-used integer notations for the chiral vector, $\mathbf{C}_{\mathrm{h}} = 20\cdot\mathbf{a}_1 + 0\cdot\mathbf{a}_2$, where $\mathbf{a}_1$ and $\mathbf{a}_2$ denote the graphene lattice vectors. The third index, 10, identifies the CNT height as $10\cdot\|\,\mathbf{T}\,\|$, where $\mathbf{T}$ is the orthogonal translational vector [19].

CNT Configuration	Atoms	Element V_{S}	p_{S}	Element V_{B}	p_{B}	Equilibrium Length
$(12,12,20)$	984	NR-2	1452	NR-3	2855	$l_0 = 48.151$ Å
$(16,8,5)$	1128	NR-2	1664	NR-3	3279	$l_0 = 53.588$ Å
$(20,0,10)$	820	NR-2	1200	NR-3	2359	$l_0 = 41.700$ Å

Table 2. CNT Model Specifications – Brittle CNT Failure Simulations

For literature comparison, the stress-strain results are reported in conventional pressure units, assuming a wall thickness $t_{\mathrm{wall}} = 3.4\,\text{Å}$, as: $\sigma_{3\mathrm{D}} = \sum f_i / A$, where f_i denotes the reaction forces at the displaced atoms, and $A = t_{\mathrm{wall}}\,\|\,\mathbf{C}_{\mathrm{h}}\,\|$. The strain is evaluated as $\epsilon = l / l_0 - 1$.

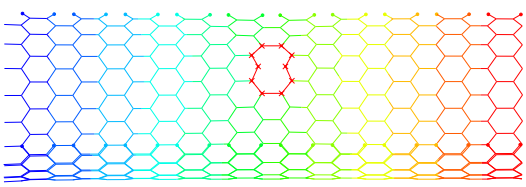

Figure 5. Cut-View of CNT $(20,0,10)$ with Highlighted Softened Bond Region in an Axial Deformation Field

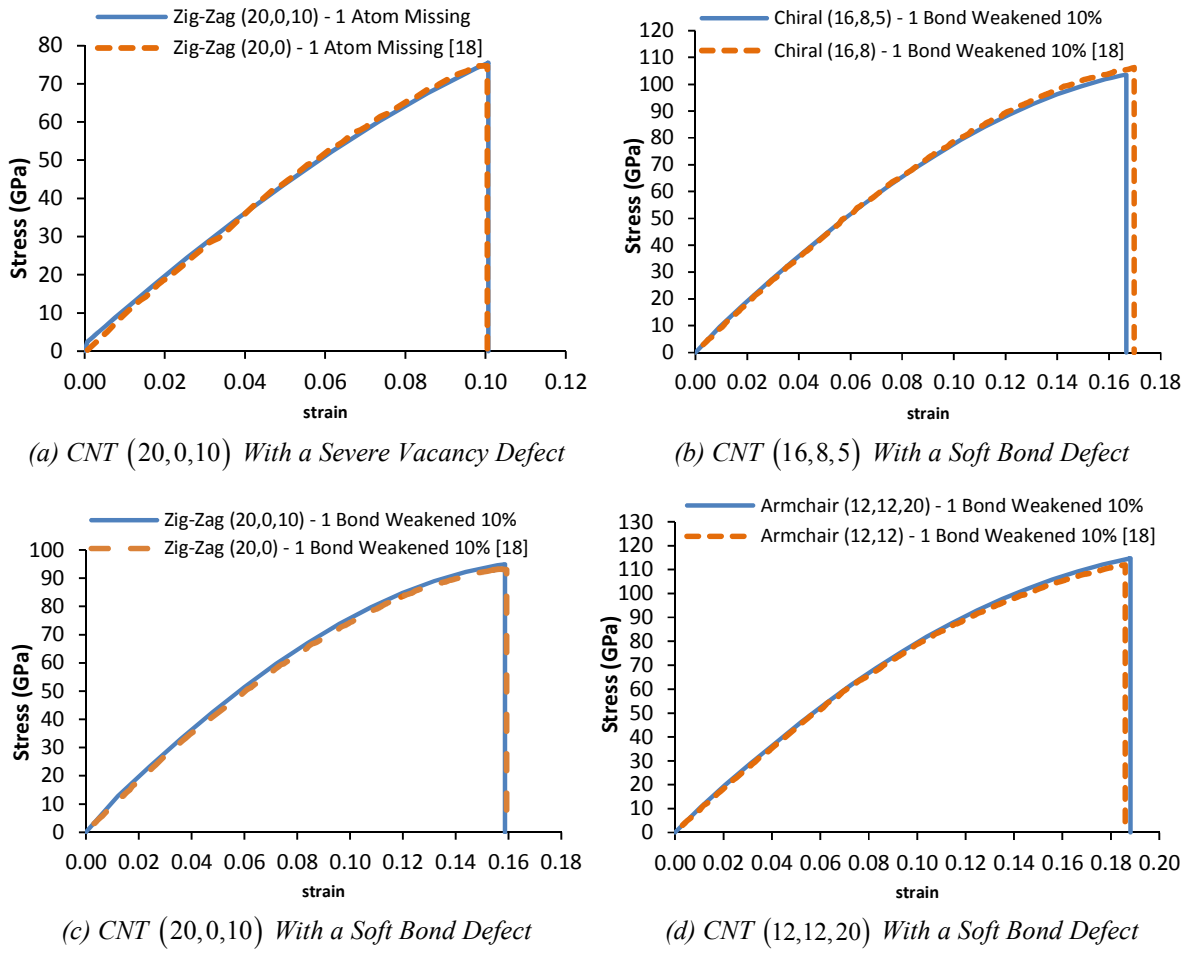

(a) CNT $(20,0,10)$ *With a Severe Vacancy Defect*

(b) CNT $(16,8,5)$ *With a Soft Bond Defect*

(c) CNT $(20,0,10)$ *With a Soft Bond Defect*

(d) CNT $(12,12,20)$ *With a Soft Bond Defect*

Figure 6. Stress-Strain Behaviours of CNT of Varying Chirality with Defects

Figure 6 demonstrates an excellent agreement between the current MDFEM implementation and the MD results reported in [18]. The predictions for failure strain and failure stress show no identifiable differences for the Zig-Zag CNTs, while for the Chiral and Armchair CNTs these are minor and negligible. Additionally, the brittle nature of the fracture can be deduced from MDFEM because no bonds had fully failed prior to global divergence. Figure 5 highlights the domain of the CNT which surrounds the softened bond at a global axial strain of 15.8%. All simulations took $\mathcal{O}(10^1 - 10^2)$ seconds to complete using a standard workstation running a 3.3 GHz Intel i5-2500 CPU.

5.2 Conformational Analyses: 3D Pillared Graphene Structures (PGS)

The seeding of PGS meshes, such as those in figures 7(a) and 7(c), is mathematically considerably more complex and computationally intensive than seeding a SLGS or CNT [20, 21]. A conformational analysis is typically required before any loading may be applied. Two examples are presented, the first being PGS-1, figure 7(a). This PGS is constituted of a single CNT of configuration $(8,0,4)$, which is perpendicularly joined to SLGS at both its ends. The second example, PGS-2 in figure 7(b), is more complex due to the close proximity of its two CNT which are of configurations $(8,0,4)$ and $(6,0,4)$. Both the PGS-1 and PGS-2 configurations are potentially representative Unit Cell (UC) domains. These structures were equilibrated using the Lobo-Keating potential [16], with the following fitting parameters: $r_0 = 1.421\,\text{Å}$, $\alpha = 15.59\,\text{nN/Å}$, $\beta = 2.55\,\text{nN/Å}$ and $\gamma = 0.74\,\text{nN/Å}$.

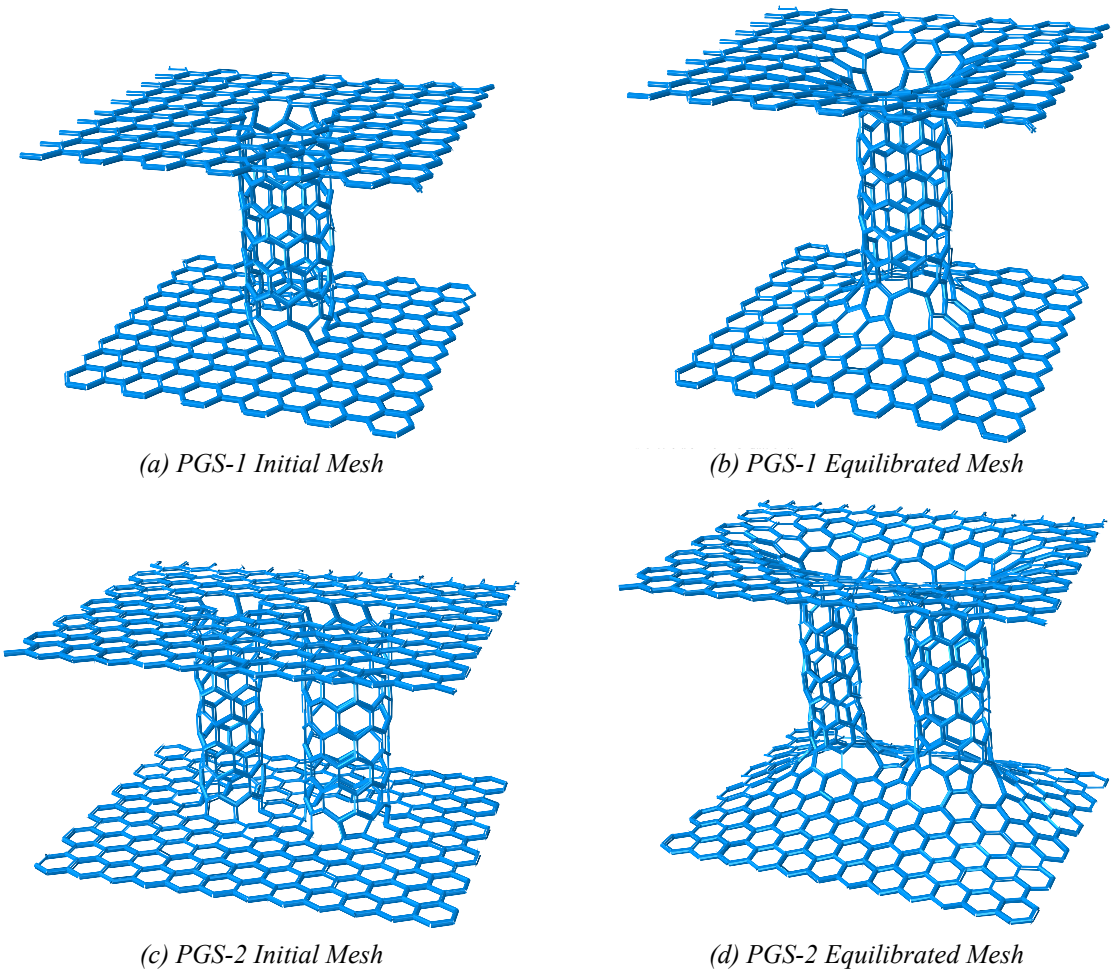

(a) PGS-1 Initial Mesh *(b) PGS-1 Equilibrated Mesh*

(c) PGS-2 Initial Mesh *(d) PGS-2 Equilibrated Mesh*

Figure 7. Conformational Analyses of Non-Equilibrium PGS Meshes

The equilibrated state of the PGS-1 in figure 7(b) and that of PGS-2 in figure 7(d), are easily obtained by prescribing $\mathbf{f} = \mathbf{0}$ and appropriate basic boundary conditions on the structures, which allow the geometries to relax to their energy minimizing configuration.

Homogenized mechanical properties of PGS, obtained through an approximated MDFEM, are available by Sihn et al. [11], but the latter study required a full MD pre-processing step to obtain the conformational analysis prior to loading. It is recommended that only force fields with strictly monotonic force-displacement relations (i.e. inflexion-free potentials) be used in conformational analyses. This criterion almost always guarantees fast, problem-free convergence to an approximate energy minimum, which may be refined with a more precise force field around that energy minimum. Figure 7(d) demonstrates that the current MDFEM is able to perform conformational analyses on quite challenging geometries.

6 Conclusions

A mathematically rigorous, fully non-linear Molecular Dynamic Finite Element Method (MDFEM) has been presented. The model has shown to yield numerical predictions identical to MD fracture simulations and has produced, to the best of the authors' knowledge, novel results by achieving the first fully MD-equivalent conformational analyses performed within MDFEM. The formulation bases itself on the simplest possible MDFEM element topologies which are available throughout literature, and hence the force field characteristic variables are defined unambiguously. This intuitive and clear approach significantly facilitates the numerical implementation of MDFEM and should spark an increased use of the latter.

The symbolic derivatives of the elements' Jacobian and Hessian applied in this work, only requires the force field in its basic form, $V = V(\mathbf{c})$, and an appropriate choice of element topologies defining the characteristic variables, $\mathbf{c} = \mathbf{c}(\mathbf{x}, \mathbf{u})$, in order to model the chosen MD force field exactly within MDFEM. Finally, the current model is ideally suited for multi-scale integration (hierarchical and concurrent) with larger-scale FEM simulations. Due to its formal derivation, the current MDFEM may equally accommodate multi-physics effects if the element topologies are enriched with appropriate DoF beyond the current displacements.

Acknowledgements
The present project is supported by the National Research Fund, Luxembourg (1360982). Roshan Bhalla is acknowledged for generating the PGS meshes.

References

[1] R. A. Barton, J. Parpia, and H. G. Craighead. "Fabrication and performance of graphene nanoelectromechanical systems". *Journal of Vacuum Science & Technology B: Microelectronics and Nanometer Structures*, **29**, pp. 050801 (2011).
[2] I. Pettersson and T. Liljefors. *Molecular Mechanics Calculated Conformational Energies of Organic Molecules: A Comparison of Force Fields*. pp.167–189, John Wiley & Sons, Inc. (2007).
[3] D. Srivastava and et al. "Computational nanotechnology: A current perspective". *CMES*, **3**, pp. 531–538 (2002).
[4] R. Car and M. Parrinello. "Unified approach for molecular dynamics and density-functional theory" *Phys. Rev. Lett.*, **55**, pp. 2471–2474 (1985).
[5] D. W. Brenner. "Empirical potential for hydrocarbons for use in simulating the chemical vapor deposition of diamond films". *Phys. Rev. B*, **42**, pp. 9458–9471 (1990).
[6] G. M. Odegard, T. S. Gates, L. M. Nicholson, and K. E. Wise. "Equivalent-continuum modeling of nano-structured materials". NASA Technical Report, NASA/TM-2001-210863 (2001).
[7] C. Li and T.-W. Chou. "A structural mechanics approach for the analysis of carbon nanotubes". *International Journal of Solids and Structures*, **40**, pp. 2487 – 2499 (2003).
[8] B. Liu, Y. Huang, H. Jiang, S. Qu, and K. Hwang. "The atomic-scale finite element method". *Computer Methods in Applied Mechanics and Engineering*, **193**, pp. 1849 – 1864 (2004).
[9] L. Nasdala and G. Ernst. "Development of a 4-node finite element for the computation of nano-structured materials". *Computational Materials Science*, **33**, pp. 443 – 458 (2005).
[10] T. C. Theodosiou and D. A. Saravanos. "Molecular mechanics based finite element for carbon nanotube modeling". *ASME Conference Proceedings*, pp. 55–64 (2006).
[11] S. Sihn, V. Varshney, A. K. Roy, and B. L. Farmer. "Prediction of 3d elastic moduli and poisson's ratios of pillared graphene nanostructures". *Carbon*, **50**, pp. 603 – 611 (2012).
[12] L. Nasdala, A. Kempe, and R. Rolfes. "The molecular dynamic finite element method (mdfem)". *CMC*, **19**, pp. 57–104 (2010).
[13] L. Nasdala, A. Kempe, and R. Rolfes. "Are finite elements appropriate for use in molecular dynamic simulations?". *Composites Science and Technology* (2012).
[14] J. Wackerfuß. "Molecular mechanics in the context of the finite element method". *International Journal for Numerical Methods in Engineering*, **77**, pp. 969–997 (2009).
[15] N. L. Allinger, Y. H. Yuh, and J. H. Lii. "Molecular mechanics. the mm3 force field for hydrocarbons. 1". *Journal of the American Chemical Society*, **111**, pp. 8551–8566 (1989).
[16] C. Lobo and J. L. Martins. "Valence force field model for graphene and fullerenes". *Zeitschrift für Physik D Atoms, Molecules and Clusters*, pp. 159–164 (1997).
[17] A. Rappé and C. Casewit. *Molecular Mechanics Across Chemistry*. University Science Books (1997).
[18] T. Belytschko, S. P. Xiao, G. C. Schatz, and R. S. Ruoff. "Atomistic simulations of nanotube fracture". *Phys. Rev. B*, **65**, pp. 235430 (2002).
[19] M. Dresselhaus, G. Dresselhaus, and R. Saito. "Physics of carbon nanotubes". *Carbon*, **33**, pp. 883 – 891 (1995).
[20] H. Terrones and A. Mackay. "The geometry of hypothetical curved graphite structures". *Carbon*, **30**, 1251 – 1260 (1992).
[21] D. Baowan, B. J. Cox, and J. M. Hill. "Two least squares analyses of bond lengths and bond angles for the joining of carbon nanotubes to graphenes". *Carbon*, **45**, pp. 2972 – 2980 (2007).